Since January 2020 Elsevier has created a COVID-19 resource centre with free information in English and Mandarin on the novel coronavirus COVID-19. The COVID-19 resource centre is hosted on Elsevier Connect, the company's public news and information website.

Applied Soft Computing 138 (2023) 110210

Contents lists available at ScienceDirect

Applied Soft Computing

journal homepage: www.elsevier.com/locate/asoc

Density estimation of SARS-CoV2 spike proteins using super pixels segmentation technique

Bakr Ahmed Taha [a], Qussay Al-Jubouri [b], Yousif Al Mashhadany [c], Mohd Hadri Hafiz Mokhtar [a], Mohd Saiful Dzulkefly Bin Zan [a], Ahmad Ashrif A. Bakar [a], Norhana Arsad [a,*]

[a] UKM—Department of Electrical, Electronic and Systems Engineering, Faculty of Engineering and Built Environment, Universiti Kebangsaan Malaysia, UKM Bangi 43600, Malaysia
[b] Department of Communication Engineering, University of Technology, Baghdad, Iraq
[c] Department of Electrical Engineering, College of Engineering, University of Anbar, Anbar, 00964, Iraq

ARTICLE INFO

Article history:
Received 9 January 2022
Received in revised form 14 April 2022
Accepted 7 March 2023
Available online 16 March 2023

Dataset link: https://zenodo.org, https://doi.org/10.5281/zenodo.3985098, https://doi.org/10.5281/zenodo.3985110, https://doi.org/10.5281/zenodo.3986526, https://doi.org/10.5281/zenodo.3986580, https://doi.org/10.5281/zen, https://doi.org/10.5281/zendo.4275742, https://doi.org/10.5281/zendo.4275769

Keywords:
Coronaviruses
SARS-CoV 2
Superpixel technique
Segmentation
Spike proteins

ABSTRACT

The worldwide outbreak of COVID-19 disease was caused by the severe acute respiratory syndrome coronavirus 2 (SARS-CoV 2). The existence of spike proteins, which allow these viruses to infect host cells, is one of the distinctive biological traits of various prior viruses. As a result, the process by which these viruses infect people is largely dependent on spike proteins. The density of SARS-CoV-2 spike proteins must be estimated to better understand and develop diagnostics and vaccines against the COVID-19 pandemic. CT scans and X-rays have three issues: frosted glass, consolidation, and strange roadway layouts. Each of these issues can be graded separately or together. Although CT scan is sensitive to COVID-19, it is not very specific. Therefore, patients who obtain these results should have more comprehensive clinical and laboratory tests to rule out other probable reasons. This work collected 586 SARS-CoV 2 transmission electron microscopy (TEM) images from open source for density estimation of virus spike proteins through a segmentation approach based on the superpixel technique. As a result, the spike density means of SARS-CoV2 and SARS-CoV were 21,97 nm and 22,45 nm, respectively. Furthermore, in the future, we aim to include this model in an intelligent system to enhance the accuracy of viral detection and classification. Moreover, we can remotely connect hospitals and public sites to conduct environmental hazard assessments and data collection.

1. Introduction

Coronavirus diseases (COVID-19) caused by SARS-CoV 2 are spreading rapidly around the world, infecting and killing millions of people [1]. Like many worldwide disasters in human history, the disease is wreaking havoc on multiple countries' health and economic systems. As a result, the Centers for Disease Control and Prevention (CDC) have outlawed large gatherings throughout the world, including all types of social activities, schools, and festivals [2–4]. Many viruses pose a significant public health risk, such as infected 8000 people with the severe acute respiratory syndrome coronavirus (SARS-CoV) between 2002 and 2003, killing approximately 10% of them [5,6]. More than 1700 persons were infected with the Coronavirus of Respiratory Syndrome in the Middle East (MERS-CoV) in 2012, with a fatality rate of roughly 36% [7,8]. In 2020, according to the last update to the Johns Hopkins University Center for Systems Science and Engineering, Coronavirus disease (COVID-19) caused 226,870,408 infections worldwide and 4,666,053 deaths [9]. These viruses have a spike structure that protrudes from a spherical surface [10], a strong affinity potential for cells and environmental mobility simultaneously. Biological and colloidal research has revealed that the viral spikes protein of SARS-CoV-2 is responsible for the entry, attachment and fusion of cells during viral infection [10]. In this study a strong relationship has been reported between the D614G mutation in the SARS-CoV-2 spike protein and increased infections and virion density [11]. Virus spikes enable virus attachment to surfaces through receptor-specific interactions (RSIs), facilitate membrane fusion, and define or alter viral tropism. These structure-function correlations have important

* Corresponding author.
E-mail addresses: p103537@siswa.ukm.edu.my (B.A. Taha), qussay.s.tawfeeq@uotechnology.edu.iq (Q. Al-Jubouri), yousif.mohammed@uoanbar.edu.iq (Al Mashhadany), hadri@ukm.edu.my (M.H.H. Mokhtar), saifuldzul@ukm.edu.my (M.S.D.B. Zan), ashrif@ukm.edu.my (A.A.A. Bakar), noa@ukm.edu.my (N. Arsad).

https://doi.org/10.1016/j.asoc.2023.110210
1568-4946/

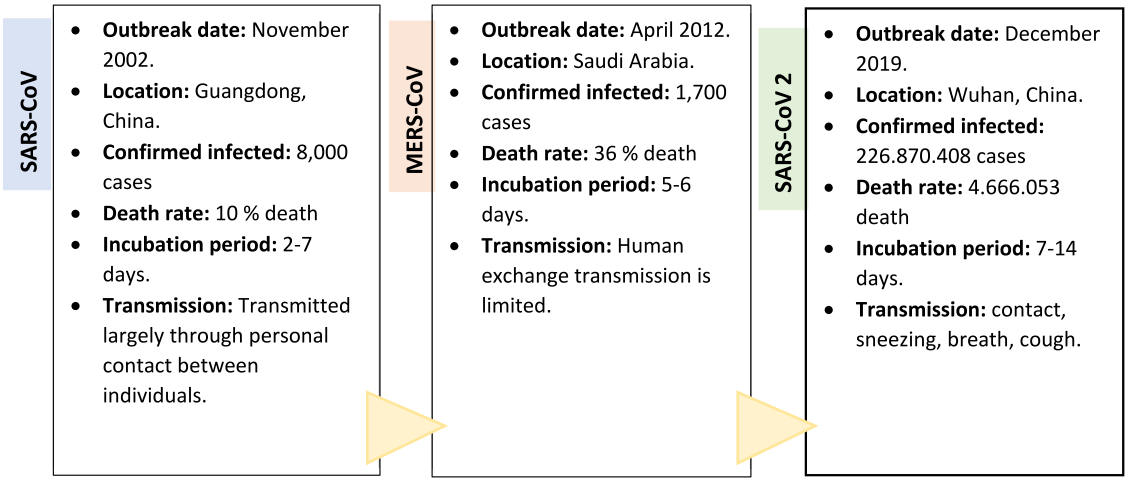

Fig. 1. Comparison between SARS-COV, MERS-COV, and SARS-COV 2.

implications for creating virus-like particles and colloids, which will aid in the development of antiviral vaccines and drug delivery applications [12,13]. Different virus detection results from image data shows that Spike proteins are critical morphological elements for categorizing viral electron microscope images and indistinguishable spikes for similarities with background noise. Accordingly, both SARS and COVID-19 contain highly infectious spike proteins [14]. Recent results suggest that a mutation change in COVID-19 is spreading across Europe and the United States, leading to higher infectivity and stability of the virus. This trivial difference would significantly improve the spike receptors and allow the virus to attach to and infect cells. In general, minor genetic changes occur as viruses reproduce and spread, but these changes have minimal impact on fitness or competitiveness; This SARS-CoV 2 mutation, missing during the first regional pandemic, appears to have taken control of most of the world [11]. Spiky proteins are used to inactivate viruses and prevent infections, and nanoparticles with core lengths of around 120 nm and diameters of approximately 30 nm are created. The creation of spiky topography inhibitors improves the interactions between viruses and inhibitors [15]. According to a recent study, the probability of virus size distribution without spikes is about 100 nm, and both viruses had a maximum spike length of 23 nm. However, the number of spikes per virus particle in SARS-CoV was approximately 30% more than in SARS-CoV 2 [15]. In contrast, another variant of the SARS-CoV virus is estimated to have an average of 50,100 spikes per virion [16]. However, these images allow clinicians to better understand the internal structures and to understand the dimensions, structure, density, texture, and shape of the internal structures. Object recognition algorithms recognize the occurrence of a certain type of object by combining the retrieved properties using learning processes. However, feature extraction is the process of identifying and interpreting the things that are important to a particular situation and developing a tool to recognize those features. A thorough knowledge of the framework or problem enables you to make informed decisions about which features could be useful in many situations. Fig. 1 shows the comparison with SARS-CoV, MERS-CoV, and SARS-CoV 2.

2. Research contribution

The coronavirus infection cycle begins with receptor binding and membrane fusion, which are critical. SARS-CoV 2 is covered with spike proteins. The S protein facilitates viral attachment to ACE2 as a cellular receptor during virus entry. The estimated spike protein density of SARS-CoV 2 can provide a foundation for understanding interactions between S and neutralizing antibodies during infection or immunization [17]. In this paper, we use transmission electron microscopy images of SARS-CoV 2 and SARS-CoV to examine and extract features of the density spike protein, allowing new insights into detection methods. Furthermore, as can be shown, it reduces the likelihood of a pandemic spreading. The main contribution of the research is:

- Determine density of spike protein and comparing them to SARS-CoV is important can contribute this feature to enabled diagnostic tools with artificial intelligence for identify life cycle of virus, mutations and disease progression.
- Flow chart proposed of super-pixel segmentation algorithm to estimate the density of SARS-CoV 2 spike proteins.
- We aim to combine this model with an intelligent system in future work to improve the accuracy of viral identification and detection on surfaces. This might enable us to connect hospitals and public places in order to monitor environmental dangers and gather data remotely [18–20].

3. Related studies

In recent years, super-pixels have grown increasingly useful for computer vision applications. It can also adhere to picture boundaries and speed, storage efficiency, and influence on segmentation performance [21,22]. Iterative clustering, a method based on simple linear iterative clustering, reduces the number of cells necessary for thresholding and the time required to segment pictures (SLIC). Considering the split and merge levels may accomplish numerous seeds and various seed point requirements in practice [23]. A study shows a superpixel generation technique for automatic glioma segmentation based on simple linear iterative clustering.

The results were highly consistent with expert delimitation in all glioma grades, resulting in a simple and reliable method for glioma segmentation [24]. Many studies use deep learning in detection and classification [24–27]. Researchers also developed a new SLIC-based superpixel algorithm that uses clustering of k-means to generate superpixels efficiently [21]. A faster SLIC superpixel segmentation technique that efficiently reduces the number of candidate segments for each pixel by taking advantage of the significant spatial redundancy in natural images. Results were up to five times faster than SLIC, while achieving nearly identical super-pixel segmentation performance in terms of sub-segmentation errors and marginal memory [28]. A method for

segmenting a brain tumor from multimodal MRI images has been disclosed that uses the Walsh Hadamard Transform (WHT) texture for super pixel-based spectral clustering. It provided high quality segmentation results for brain tumor segmentation [29]. In one research, a two-step segmentation strategy was demonstrated to recover cell features from high-resolution histopathology pictures of renal cell carcinoma. Using the SLIC technique, the image is first divided into super pixels. Second, utilizing state-of-the-art clustering-based segmentation techniques, the produced super pixels are grouped to identify comparable super pixels that contain the cell nuclei [30]. Similarity coefficients of 0.92 and higher were discovered by including an edge detector into a superpixel algorithm and adapting it for multichannel images [31]. A superpixel segmentation hierarchy uses algorithms that require different visual details. However, there is no technology that can reliably synthesize all scales in real time [32,33]. But researchers are able to identify object boundaries accurately and keep the regular shape based on the super-pixel segmentation algorithm [31]. Cryo-EM imaging was used to examine the structures and distributions of the spiking proteins of SARS-CoV 2 virion morphology on intact virions. In terms of diameter, the mean and standard deviation for each of the three preparations is 911, 949, and 928 nm, respectively [17]. Many studies described the length of the viral spike protein, which was around (9–12) nm in length and gave virions the appearance of a solar corona. Furthermore, the foundation design is comparable with the coronavirus family. The presence of viral tips and membranes in cryo-EM images of isolated SARS-CoV-2 Surrounding 20% to 30% of virions contain many spines around the membrane. In contrast, most other virus particles have few spikes [34].

4. Viruses spiked

The spike protein is essential in virus entry into a human host to the receptor and cell membrane fusion. It is crucial to note that the SARS-CoV 2 spike proteins are made up of two functional subunits, the N-terminal S1 region and the C-terminal S2 region, which are found in the viral envelope. The S1 subunits of SARS-CoV and SARS-CoV 2 encompass the same as the use of the angiotensin converting enzyme 2 (ACE2) receptor in host cells as an entry fusion receptor due to the spike in viral infection. S2 acts as a transmembrane anchor during the endosomal journey and allows the fusion of virus and host cell membranes. Cell surface fusion can nevertheless occur under certain conditions [10,35,36]. The spike protein SARS-CoV 2 is essential for cell penetration and the main reason for the vaccine to grow. The research demonstrated the mixture of cryo-electron tomography, averaging of sub-tomograms, and simulations of molecular dynamics for structural depth analysis in situ. As a result, the S-stem domain has been shown to have three joints, which gives the head unpredictable flexibility of orientation. The three flexible hinges are marked with the hip, knee and ankle [37]. Particles of the virus have been shown to be roughly or slightly pleiomorphic. Although a small proportion of spikes are known, most spikes occur in the form of nails, similar to the perfusion state in which the S1 spike protein is separated from S2. Cryoelectron tomography was used to detect these spikes, which correlate extremely closely with the general structure of the SARS-CoV spikes [38]. In addition, it has been suggested that spike interacts with host factors to allow infection in addition to its role in cell entry [39]. It presented a detailed in situ investigation of the SARS-CoV 2 spike utilizing cryo-electron microscopy (Cryo-EM) to verify its various confirmations, orientations, and virion particle dispersions [40]. As mentioned earlier, the researchers used cryo-electron microscopy (cryo-EM) to uncover the intricacies of the spike protein structure on the virion's surface. It could serve as a focal point for vaccine immunogen design.

5. Mechanism of entry of the SARS-CoV 2 virus

The viral genome can penetrate the host cell to cause the fusion when the virus membrane and the host cell membrane fuse. Host proteases prevent the Spike protein SARS-CoV 2, consisting of subunits S1 and S2 separated from the remaining covalent until viral fusion occurs by splitting into S1 and S2 [38]. Consequently, the S2 subunit must undergo two crucial conformational changes during the attachment of the S1 subunit to receptors on host cells to complete the fusion of the viral membrane with the cell membrane. HR1 and HR2 are two of the S2 subunit's heptad repeat (HR) regions involved in coronavirus fusion. Therefore, it is vital to understand how viruses enter cells to keep them out. For example, human ACE2 and human proteases are utilized as entrance receptors and activators for SARS-CoV 2, respectively. As a result, the infection might spread more widely [41]. Depending on the virus type, a high glycoside content (between 1160 and 1400 amino acids) is essential for the penetration of the S protein into host cells and the commencement of infection. The presence of S proteins causes prickly protrusions on coronaviruses [42,43]. Fig. 2 illustrates possible mechanisms of spike protein amplification of infection.

6. Methodology

The aim of our study is to use superpixels as fundamental components of visual feature recognition and learning to represent objects in a future study. To achieve this purpose, the preferred approach should primarily meet the following criteria. First, the approach should be fast enough to be used in near-real-time applications. Second, clusters should have minimal intra-cluster and high inter-cluster variance. Third, stability of the cluster location in the imaging room. Fourth, the segmented super-pixel boundary should match the appropriately sized boundary and serve different pixels. Flowchart for extracting the density spike protein from SARS-CoV 2 based on the superpixel method, as shown in Fig. 3.

6.1. Data availability statement

A data set is a set of raw statistics and information obtained from a research study. Datasets created by government agencies or nonprofit groups are often available for free download. In our study, we used seven data sets recorded on the Zenodo website, a universal open access repository created under the European Open-AIRE program and maintained by CERN. It enables researchers to add research papers, data sets, research software, reports, and other digital links to their research. Each contribution is assigned a persistent digital object identification (DOI), which makes the saved objects easy to cite. We have described the collection of the data set, which includes Transmission Electron Microscopy SARS-CoV 2 and SARS-CoV images, as shown in Table 1. It comprises 586 transmission electron microscopy images of ultrathin (60−70 nm) plastic sections through extracellular virus particles in Vero cell cultures. Images captured with a resolution of 1376–1032 pixels and saved in 16-bit TIF format. In addition, an image viewer can read 16-bit images for all images in order to visualize the images (e.g. Irfan-View). Image files are size calibrated and can be opened in ImageJ or Fiji using the bioformats importer with the required size calibration.

6.2. Simple Linear Iterative Clustering (SLIC)

Super-pixel techniques are widely used in computer vision applications. It uses set criteria to process all pixels randomly,

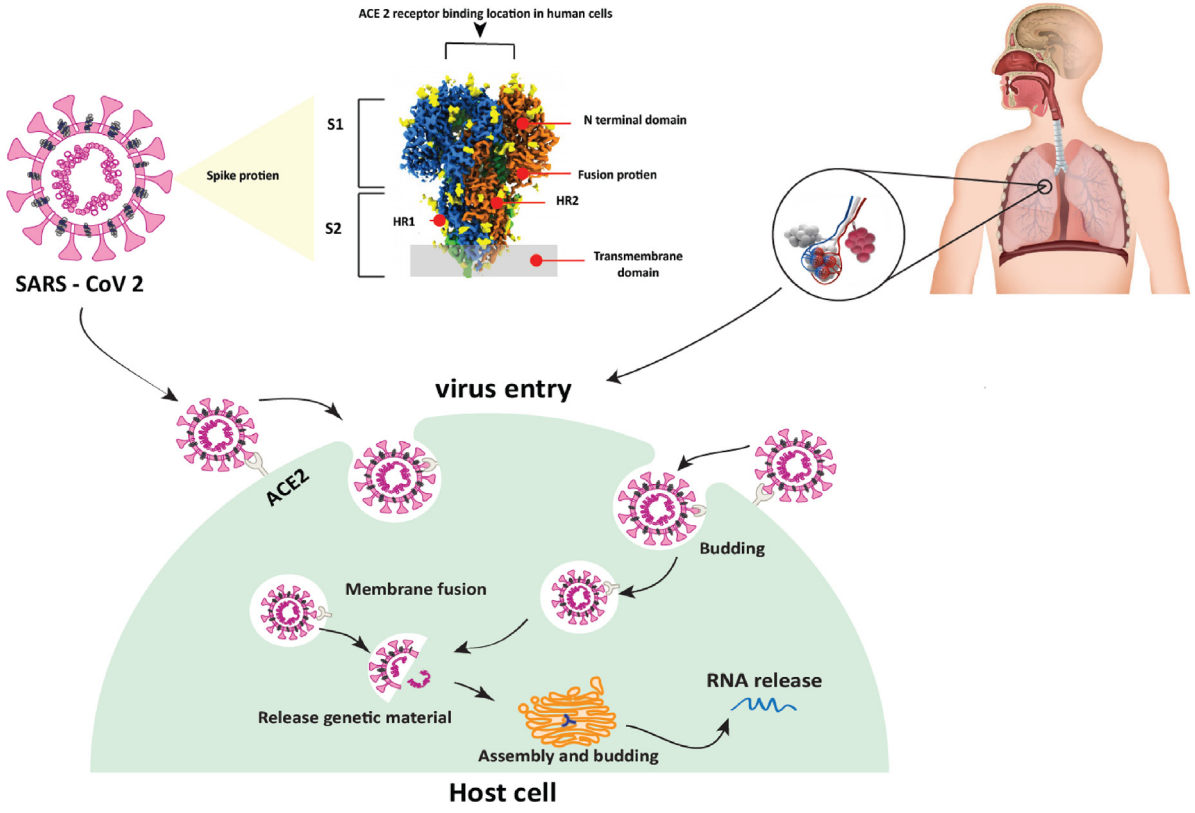

Fig. 2. Potential mechanisms of amplification of infection by the SARS-CoV 2 spike protein.

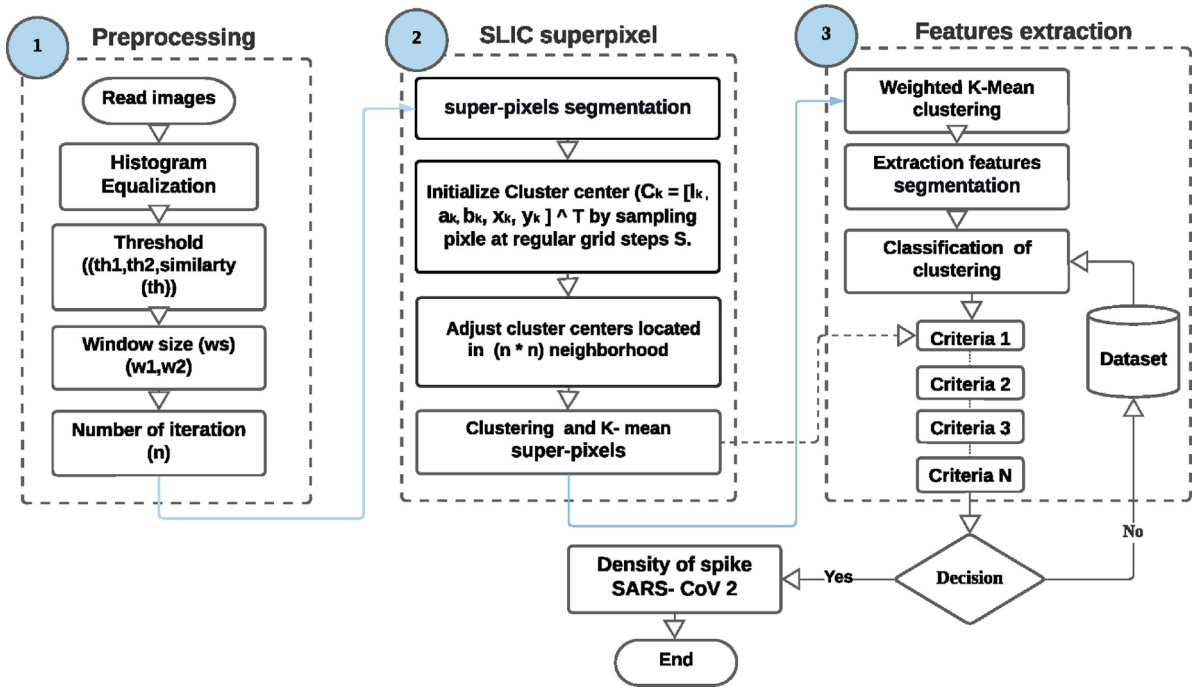

Fig. 3. Flow chart to estimate the density spike protein of SARS-CoV 2 using the superpixel segmentation technique.

Table 1
A description of the data sets that were used for the virus particles SARS-C0V2 and SARS-COV.

Data	Location of virus isolation	Virus categories	Count of images	File type	Reference
Dataset 1	Germany/Frankfurt	SARS-CoV	126	Tif, 16-bits	https://doi.org/10.5281/zenodo.3985098
Dataset 3	Italy-INMI	SARS-CoV 2	128	Tif, 16-bits	https://doi.org/10.5281/zenodo.3985110
Dataset 6	Germany/Frankfurt	SARS-CoV	111	Tif, 16-bits	https://doi.org/10.5281/zenodo.3986526
Dataset 7	Italy-INMI	SARS-CoV 2	134	Tif, 16-bits	https://doi.org/10.5281/zenodo.3986580
Dataset 10	Italy-INMI	SARS-CoV 2	66	Tif, 16-bits	https://doi.org/10.5281/zenodo.4275769
Dataset 11	Germany/Frankfurt	SARS-CoV	10	Tif, 16-bits	https://doi.org/10.5281/zenodo.4275742
Dataset 12	Italy-INMI	SARS-CoV 2	11	Tif, 16-bits	https://doi.org/10.5281/zenodo.4275769

resulting in unnecessary super-pixel boundaries and regularity [44]. A super pixel is a series of pixels that overlap certain features such as pixel intensity. It is becoming increasingly valuable to several image processing algorithms, including image segmentation, semantic labeling, object recognition, and tracking, for the following reasons: First, they provide more information than pixels. Second, they are conceptual in that pixels that correspond to the same superpixel have similar image characteristics. Third, they describe images in an efficient and compact approach that can be valuable for high-performance computing challenges [45,46]. A study shows the use of the super-pixel method to analyze histogram-corrected medical images. The two conceptual methodologies were used to determine whether a grayscale image was equalization and histogram segmentation [47]. Segmentation of an image can be considered a set of boundaries or a series of segments that span the full image. For example, the color, brightness, and texture can be the same for most of the segmented pixels, but differ dramatically between adjacent segments. Segment borders and edges tend to be closely connected, because of the considerable brightness shifts at the sections' boundaries. Therefore, a different segmentation technique is built on edge extraction methods using k-means clustering, SLIC segmentation, to group nearby pixels. Generally, the idea concept is to initialize the center of the superpixel by sampling the location (N) location on the regular grid (A) in the image plane and shifting them within $S \times S$ the SS neighborhood to seed in the position with the lowest gradient. For each cluster center m_i, calculate the distance between m_i and each pixel in (A)neighborhood of m_i. Assign pixels to the cluster (i) if the distance is better than before the value. Update the cluster as in K-means. Repeat once until convergence. Optionally, replace the colors of the pixels in each collection with the average.

6.3. Distance measure

Initially, K uses the desired number of superpixels of approximately the same size. And in the case of an image with N pixels, as a result, the approximate size of each superpixel is $N = K$ pixels. Every grid interval $S = \sqrt{N/k}$ would have a super-pixel center for nearly equal sized superpixels. At the beginning of our process, we select K super-pixel cluster centers $C_k = \left[l_k, \ a_k, b_k, x_k, y_k\right]^T$ with $k = [1, K]$ at regular grid intervals S. Because the spatial span of every super-pixel is around S^2, We might assume that pixels associated with this cluster center are located on the xy plane within a $2S \times 2S$ radius around the super-pixel center. In contrast, this is the search region for pixels closest to each cluster center. As a result, it represents the CIELAB color space and x; y pixel coordinates. The SLIC algorithm uses the CIELAB color space because it is perceptually homogeneous for tiny color differences. The distance D_s between two pixels I and j in SLIC is a composite of two distances, dc and ds, which express color and spatial closeness, respectively, as shown below in Eq. (1) [48].

$$\begin{aligned} d_c &= \sqrt{\left(l_i - l_j\right)^2 + \left(a_i - a_j\right)^2 + \left(b_i - b_j\right)^2} \\ d_s &= \sqrt{\left(x_i - x_j\right)^2 + \left(y_i - y_j\right)^2} \\ D &= \sqrt{\left(\frac{d_c}{m}\right)^2 + \left(\frac{d_s}{S}\right)^2} \end{aligned} \tag{1}$$

where D_s is the sum of the lab and xy plane distances normalized by the grid spacing S. A variable m is introduced in D_s which allows us to regulate the density of a super-pixel the greater the value of m, the greater the emphasis on spatial closeness and the denser the cluster. We suggest that the pixel pitch metric be given an extra score. d'_s indicates the presence of edges between two pixels, implying that an object boundary will most likely fall between the two spots. Before beginning superpixel creation, an edge detection algorithm produces a value pi for each pixel I, indicating its likelihood of being on boundary. The distance de between two pixels I and j and is then determined as the highest edge probability over all pixels on the line connecting the pixels I and j. The new distance is calculated as follows in Eq. (2).

$$\begin{aligned} d'_c &= \sqrt{\left(c_i - c_j\right)^2 + \left(y_i - y_j\right)^2 + \left(r_i - r_j\right)^2} \\ d_s &= \sqrt{\left(x_i - x_j\right)^2 + \left(y_i - y_j\right)^2} \\ d_e &= \max pt \\ D' &= \sqrt{(d'_c/m)^2 + (d_s/S)^2 + \alpha \times (d_e)^2} \end{aligned} \tag{2}$$

In super-pixel production, all of the super-pixels within the image must be connected to form an edge. The chi-square (X^2) histogram distance [7] is the similarity metric used in our technique to judge whether two neighboring super-pixels should be merged. X^2 denote the distance between two histograms P and Q is defined in Eq. (3).

$$X^2(P, Q) = \frac{1}{2} \sum_k \frac{(P_k + Q_k)^2}{P_k - Q_k} \tag{3}$$

6.4. Segmentation based super pixel

Image segmentation is the process of splitting up a digital image into a lot of small parts. This methodology seeks to simplify and change the representation of the image to make it easier to evaluate [49]. Conventional approaches frequently begin with the manual selection of elements and boundaries such as curves, lines, etc. The super-pixel approach has emerged as the most cutting-edge method for automatic segmentation. The implementation of the Simple SLIC algorithm results in a significant decrease in processing resources compared to conventional segmentation approaches and algorithms. The purpose of

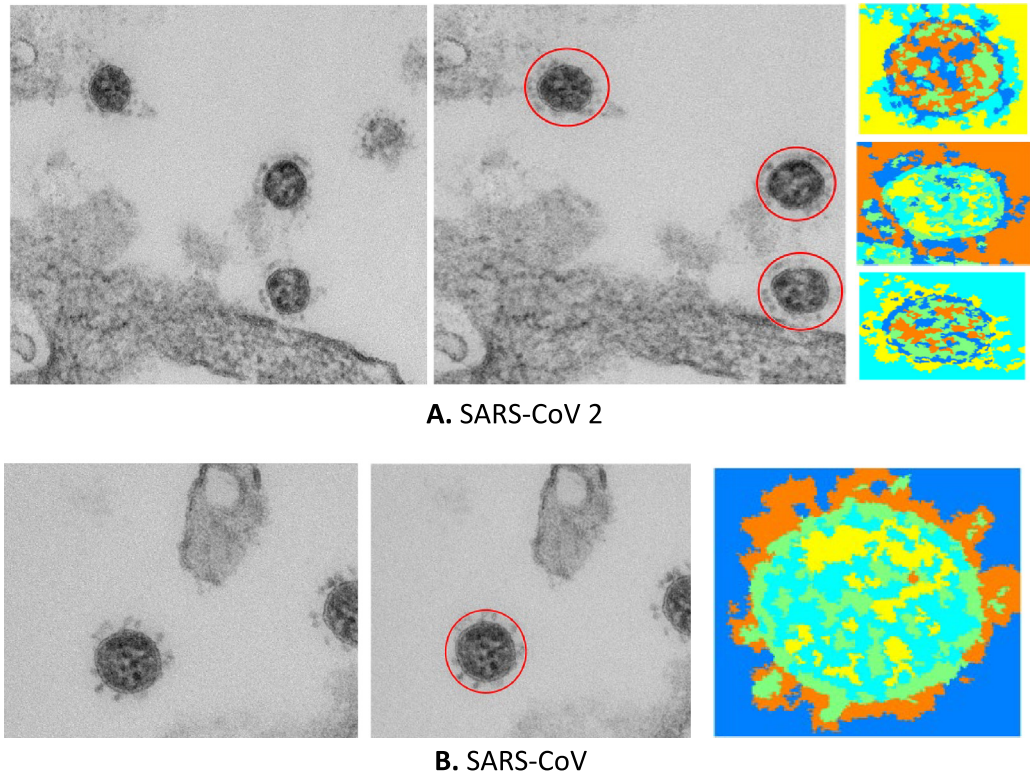

Fig. 4. Virus identification based on super pixel Segmentation using MATLAB software 2020: A. SARS-CoV 2: Dataset_08_SARS-CoV-2_006. B. SARS-CoV: Dataset_06_SARS-CoV_011.

this algorithm can be characterized as grouping image pixels in the combined five-dimensional color and picture plane space to produce compact, almost uniform superpixels successfully [50]. Segments often correlate with different types of tissue, tissues, illnesses, or structural forms that are physiologically relevant in medical imaging. This type of lung cancer segmentation is shown with low contrast increasing noise factors and other imaging locations with ambiguity. As a result, various computer-aided segmentation approaches for medical picture analysis have been developed. In this domain, sampling procedures are used; nevertheless, their application is dependent on the doctors' specific skills in the relevant methodology [51,52]. SLIC segmentation provides the same compactness; additionally, the user can specify the needed values for all super-pixels in an image. SLIC produces smooth super-pixels with regular soft sections in texturing regions, although these super-pixels are highly erratic. It is only possible if certain portions of the image fade, while others are very textured. Finding the best settings for each image can be challenging [22]. Fig. 4 shows an example of the detection of the SARS-CoV 2 virus based on the SLIC algorithm with MATLAB 2020. It can automatically choose the optimal number of super-pixels for an image, resulting in fewer super-pixels better suited to the region of interest (ROI) limits. Similarly, we generate a training set for each super-pixel by calculating its statistical texture, curvature, and fractal features. Also included is classification using clustering and segmentation.

6.5. Clustering based on K-mean

Clustering based on the K-Mean strategy of unsupervised learning was used to optimize target recognition functionality [53]. The advantages of K-mean clustering are that it is straightforward, adaptable, and easy to learn and run. Furthermore, the disadvantages of the K-mean clustering require that the number of clusters be determined in advance [53]. An approach showed a text clustering technique with multiple objectives based on the K-mean algorithm. The results show that the proposed method outperforms the other measures in terms of text clustering performance, as measured by two standard clustering measures, accuracy and F-measure [49]. The super-pixel method is based on clustering and provides performance and analysis results for a data set. As a result, the boundary detection between the super-pixel boundary and the image boundary has been improved [54,55]. However, the idea of K-mean clustering gathers N-D data into natural cluster use cluster K, the algorithm works as follows:

- specifying an initial set of cluster center $m_1 \ldots\ldots m_k \in IR^n$.
- For each $x_i \in IR^n$ in the dataset, assign it to closet cluster $x_i \in$ cluster j if $\|x_i - m_j\| < \|x_i - m_k\|\ k \neq j$.
- Update the means m_j equal average value of all x in cluster $j = \frac{1}{|C_j|} \sum_{x_{i \in C_j}} x, j = 1, \ldots, k$.
- Keep alternating 2 and 1 until m_j stop changing.

6.6. SLIC extraction feature

We represent images at the super-pixel rather than the pixel level to reduce complexity and increase the matching accuracy. Super-pixels are images that have been over-segmented as a result of the pixel clustering process. They can reflect reality more organically and more meaningfully perceptually [56]. It is able identify objects in an image with heterogeneous super-pixels and deep fold features through relationship analysis. It is

shown that it is possible to learn super-pixel properties using capsules and that performing image analysis can be useful in this organized approach. This unique deep learning architecture is assessed in the context of an image classification problem, emphasizing that the decision making of the network is explicitly interpretable [53,57]. Assume a pixel set V that is split into numerous discontinuous sections and contains all of the pixels of an image x. Each discontinuous region is assigned an aggregate value across region R, resulting in a super pixel representation of the feature space using Eq. (2) [58].

$$y_i = \frac{\sum p \in R_j \;\; x(p)}{\left|R_j\right|} \tag{4}$$

where R was chosen to account for the part-to-whole connections of the image, features are restructured to account for substructures, thereby increasing structural awareness. The relationship between the vectors of the feature space and their placement in the image is retained with this rearrangement. There are four types of segmentation algorithms: region-based, edge-constrained, classification or clustering, and some hybrid approaches [59]. Finally, the idea of K clustering means that it accepts n-dimensional data in natural clusters, in which case the user chooses k, from the cluster. In addition, we can categorize the area of the virus shape based on the color segmentation of the super pixels. The segmentation result is obtained by repeatedly adding adjacent to the cluster centers using a similarity score. Region growth algorithms are a typical representation of region-based approaches, with the essential aspects being the construction of comparable measurements and growth criteria [59]. This type of segmentation applies clustering to categorize arbitrary areas and trains classifiers based on the properties obtained from each super-pixel [60]. However, the brightness distance at the edge position is considerable in super-pixel clustering. As a result, the edge is positioned in the high brightness zone, making the segmentation results more accurate.

7. Results and discussion

Coronaviruses are responsible for the spread of epidemics such as SARS, MERS, and COVID-19. Spike proteins work in the same way as shape-changing lockpicks. It can change shape by interacting with a receptor on the surface of human cells. Spike proteins help the virus attach to and access a cell [61]. On the other hand, the cryo-electron microscopy (cryo-EM) structure of the SARS-CoV 2 spike showed that its RBD lies mainly in it, which is related to poor receptor binding. Moreover, contradictory results on the binding affinities of hACE2 for SARS-CoV 2 and SARS-CoV spikes have been published [62,63]. However, the continued rapid transmission and worldwide spread of COVID-19 has led to fascinating questions as to whether synonymous mutations, deletions and/or substitutions affect the development and adaptation of SARS-CoV-2 [64]. Recently, an approach proposed by Zunlong et al. which takes advantage of the structures, conformations, and distributions of spikes in virions, was used to understand how spike proteins function and interact with the immune system. On the virion surface, we use cryo-EM techniques to study the structure of S-trimers in situ. However, the methods lack validation and are not helpful since COVID-19 disease requires highlights such as automated identification to estimate the peak protein density, rapid diagnosis and remote control. Deep learning models are used in medical imaging approaches to extract features automatically or through pre-trained networks. After several layers have been removed, a pre-trained neural network is converted into a feature extraction technique. This redesigned network is used to configure a learning transfer process. Learning transfer expands a new challenge of machine learning by transferring knowledge from a previously perfected equivalent [17,65]. In this paper, we proposed to estimate the density of SARS-CoV and SARS-CoV 2 spike proteins using a superpixel method. First, we calculate the superpixel of the images. Second, identify the median color of each superpixel region in the plane distances color space. Third, find cluster the color feature of each superpixel using image segmentation and k- means function. Image segmentation is the process of dividing an image into groups of linked regions that are homogeneous and cohort of pixels or superpixels. Orange, blue, and yellow, for example, are made up of various clustering and segmentation sizes. The ability of the method to process a wide range of cell sizes and morphologies in TEM images recommends that it could help assess COVID-19 outbreaks. Fig. 5, Illustrate samples that were taken for each image tested in this study based on super-pixel segmentation techniques to estimate the density of spikes protein for SARS-CoV 2, and SARS-CoV using MATLAB software 2020.

The entire image is divided into regions containing essential elements or objects. The resulting things make it easier to reduce the appearance to its necessary features, making it easier to identify boundaries and objects like curves and lines. For example, superpixels are brighter and more uniformly colored regions of an impression than normal pixels, found in the polygonal portion of the image of the digital image. Therefore, computability is a crucial advantage of using superpixels [66]. Removing the highlight and shadow improves the efficiency of both image properties and features. In comparison to pixel representation, superpixel representation reduces the number of image independences. Furthermore, superpixel segmentation provides excellent support for computing regions that rely on image features, while changing the image representation to be more significant and easier to analyze [45]. The Gaussian distribution is used to estimate the density of the SARS-CoV 2 spike protein. This enables virus development to be identified using the standard deviation and width of the Gaussian. Many studies show that the mutation of a virus occurs in the spike protein [67,68]. Therefore, it is important for biologists to understand the rate of change in the peak of the spike protein. Additionally, it helps to improve the accuracy of the classification of the virus family. According to the variables of the probability density function, μ is mean, σ^2 variance (standard deviation), definitive covariance matrix. A multivariate Gaussian distribution represents each of the input objects that we are interested in a grouping. It is possible to estimate the contradiction between two Gaussians by comparing their relative entropy to represent the relative differential complexity between the two multivariate Gaussians, as an expression in Eq. (3). [69].

$$N\left(x, \mu, \sigma\right) = \frac{1}{\sqrt{2\pi\sigma}} \exp\left[-\frac{1}{2}\left(x-\mu\right)^2/\sigma^2\right] \tag{5}$$

We examined the spike distribution of the SARS-CoV and SARS-CoV-2 virus particles using TEM images and electron tomography in Vero cell cultures. Both virus isolates, SARS-CoV Frankfurt 1 and SARS-CoV-2 Italy-INMI1, were almost comparable in terms of ultrastructure and particle size distribution [70,71]. As a result, the putative processes responsible for mutations and the life cycle of the virus are revealed. The size distribution and median derived from measuring virus particle profiles in conventional ultra-thin slices may be skewed due to an overrepresentation of virus slice profiles of a particular virus particle size and undetected deformed particles. As a result, deformed virus particles (not circular/oval) were eliminated. Fig. 6 show estimates of the distributions of spikes protein using TEM images on the virion surfaces and comparisons of the distributions of density of spike proteins between SARS-CoV-2 and SARS-CoV. The results of this analysis were 21.97 nm and 22.45 nm for the mean density of SARS-CoV 2

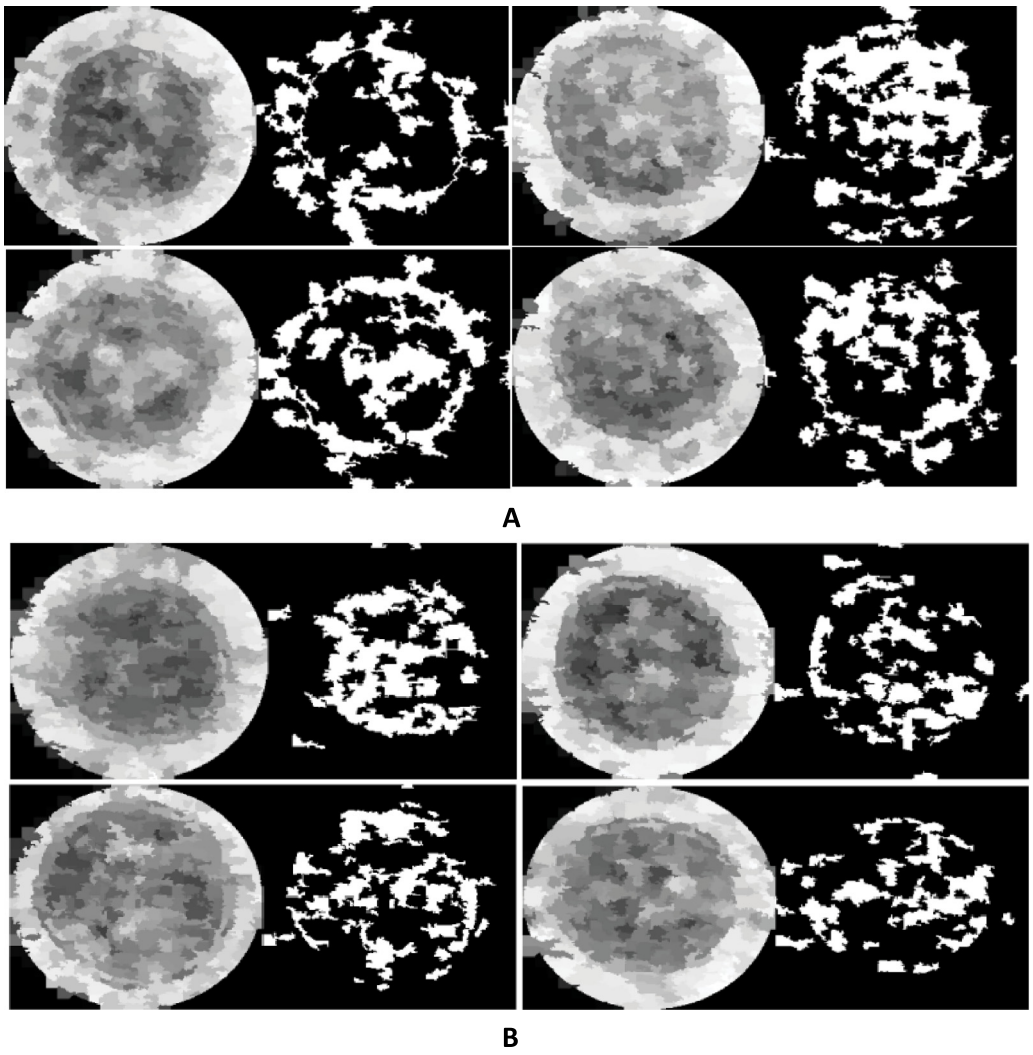

Fig. 5. Extraction density of spikes based on superpixel segmentation: A. SARS-CoV 2 and B. SARS-CoV.

and SARS-CoV spike protein, sequentially. The spike protein density of SARS-CoV-2 is actually lower when compared to SARS-CoV, which means that SARS-CoV spike protein has more spikes per virion. The standard deviation after distribution showed 6.44 nm of SARS-CoV 2 and 6.83 nm of SARS-CoV. Finally, our study was designed to guide ultrastructural work on virus-infected embedded cells. Due to their close relationship in taxonomy, showed a striking similarity in appearance and size. In contrast to non-enveloped viruses, which tend to be more uniform in size and shape, the size distribution of the two coronaviruses examined was strikingly comparable. Finally, for implicit detection, this work focuses on the super-pixel plane rather than the pixel-grid plane. It represents homogeneous regions by combining local intensity and position information; therefore, features extracted at the superpixel level can better describe the differences in local regions. In addition, super pixels preserve the image boundaries as their boundaries closely match the actual image.

8. Conclusion

The COVID-19 disease pandemic began in Wuhan and spread to almost every country. With high transmission rates and a major threat of serious disease and death among high-risk populations such as the elderly or immunosuppressed, several countries have been forced to impose rigorous measures to prevent the disease from spreading. Furthermore, this included mandatory face masks, closing public venues, and even full lockdown for staying at home. However, rapid and effective detection is required to estimate the SARS-CoV 2 spike protein density to develop diagnostics and vaccines. In this study, the results provide insight into intervention options that target cell entry mechanisms and estimate the density of spike proteins. Consequently, spikes density means of SARS-CoV2 and SARS-CoV were 21.97 nm and 22,45 nm, respectively. These findings give information on the determined average of Spike density for both viruses on the virion and offer a foundation for understanding interactions between S and neutralizing antibodies during infection or vaccination, identifying the virus's life cycle, mutations, and disease progression. In future work, we plan to establish an optical sensor based on Virus Image - Corroborated by Features Extraction to virus diagnostic. In addition, linking between hospitals and public places to provide an early warning system remotely and improve health care quality in the environment.

CRediT authorship contribution statement

Bakr Ahmed Taha: Wrote the initial manuscript draft. **Qussay Al-Jubouri:** Conceptualization, Methodology. **Yousif Al Mashhadany:** Investigation. **Mohd Hadri Hafiz Mokhtar:** Validation. **Mohd Saiful Dzulkefly Bin Zan:** Validation. **Ahmad Ashrif A. Bakar:** Validation. **Norhana Arsad:** Supervision, Validation.

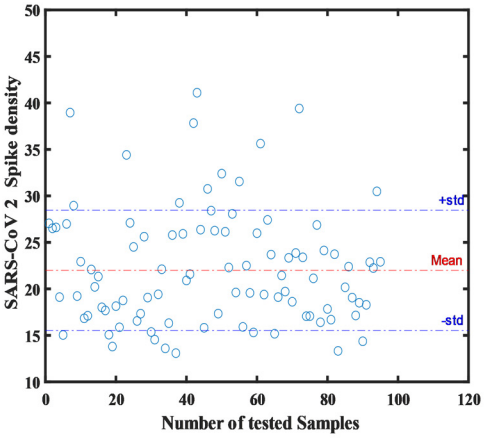

A1. Distribution density of spike protein in SARS-CoV-2 samples

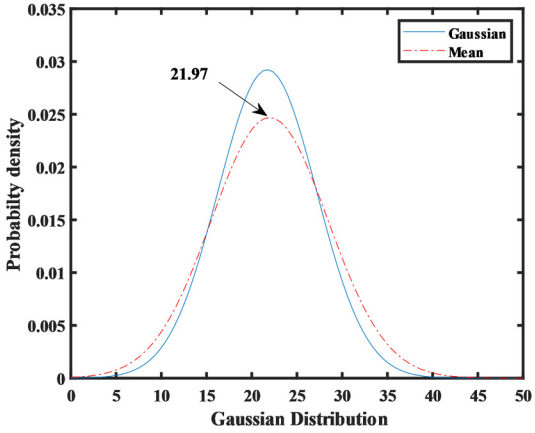

A2. Gaussian distribution of SARS-CoV-2

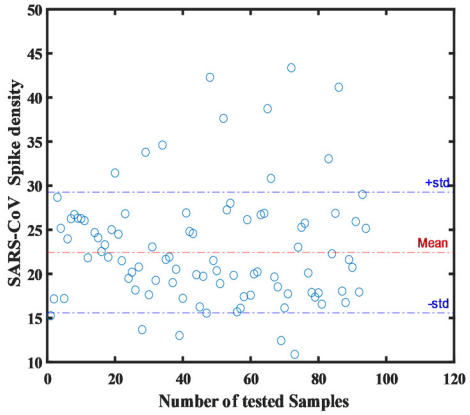

B1. Distribution density of spike protein in SARS-CoV samples

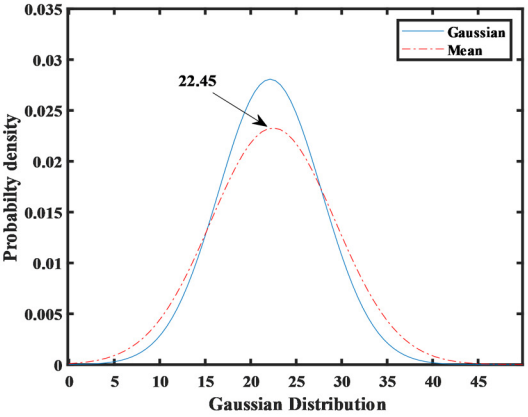

B2. Gaussian distribution of SARS-CoV

Fig. 6. Distribution of average density of spike (S) protein on the virion surfaces in TEM images: A1. density of spike protein in SARS-CoV-2, A2. Gaussian distribution of SARS-CoV-2, B1. density of spike protein in SARS-CoV, B2. Gaussian distribution of SARS-CoV.

Declaration of competing interest

The authors declare that they have no known competing financial interests or personal relationships that could have appeared to influence the work reported in this paper.

Data availability

Datasets are accessible in the Zenodo data repository: https://zenodo.org: Dataset1:https://doi.org/10.5281/zenodo.3985098; Dataset3:https://doi.org/10.5281/zenodo.3985110; Dataset6:https://doi.org/10.5281/zenodo.3986526; Dataset7;https://doi.org/10.5281/zenodo.3986580; Dataset 10: https://doi.org/10.5281/zen. Dataset 11: https://doi.org/10.5281/zendo.4275742; Dataset 12: https://doi.org/10.5281/zendo.4275769.

Acknowledgments

The authors gratefully acknowledge the financial support of the Department of Electrical, Electronic and Systems Engineering/Faculty of Engineering and Built Environment/Universiti Kebangsaan Malaysia (UKM) for their encouragement and grant support (FRGS/1/2021/TK0/UKM/02/17) and (TAP-K013436).

All authors have reviewed and accepted the published version of the manuscript.

Ethics and permission to participate

This manuscript has not been previously released and is not now under consideration by any journal for publication.

Abbreviations:

Abbreviation	Description
COVID-19	Coronavirus disease
SARS-CoV 2	Coronavirus Severe Acute Respiratory Syndrome 2
TEM	Transmission Electron Microscopy
ACE2	Angiotensin-Converting Enzyme 2
HR	Heptad Repeat
SLIC	Simple Linear Iterative Clustering
SARS-COV	Severe Acute Respiratory Syndrome Coronavirus
MERS-COV	Middle East Respiratory Syndrome Coronavirus
RSIs	Receptor-Specific Interactions
hACE2	Higher Angiotensin-Converting Enzyme 2
RBD	Receptor-binding domain

References

[1] C.C. Lai, T.P. Shih, W.C. Ko, H.J. Tang, P.R. Hsueh, Severe acute respiratory syndrome coronavirus 2 (sars-cov-2) and coronavirus disease-2019 (COVID-19): The epidemic and the challenges, Int. J. Antimicro. Ag. 55 (2020) 105924, http://dx.doi.org/10.1016/j.ijantimicag.2020.105924.

[2] S.R. Baker, N. Bloom, S.J. Davis, K. Kost, M. Sammon, T. Viratyosin, The unprecedented stock market reaction to COVID-19, Rev. Asset Pricing Stud. 10 (2020) 742–758, http://dx.doi.org/10.1093/rapstu/raaa008.

[3] S.S. Enitan, I.N. Ibeh, A.S. Oluremi, A.O. Olayanju, G.E. Itodo, The 2019 novel coronavirus outbreak: Current crises, controversies and global strategies to prevent a pandemic, Int. J. Pathog. Res. 4 (2020) 1–16, http://dx.doi.org/10.9734/ijpr/2020/v4i130099.

[4] R.C. Chick, G.T. Clifton, K.M. Peace, B.W. Propper, D.F. Hale, A.A. Alseidi, T.J. Vreeland, Using technology to maintain the education of residents during the COVID-19 pandemic, J. Surg. Educ. 77 (2020) 729–732, http://dx.doi.org/10.1016/j.jsurg.2020.03.018.

[5] P.A. Rota, M.S. Oberste, S.S. Monroe, W.A. Nix, R. Campagnoli, J.P. Icenogle, S. Peñaranda, B. Bankamp, K. Maher, M. hsin Chen, S. Tong, A. Tamin, L. Lowe, M. Frace, J.L. DeRisi, Q. Chen, D. Wang, D.D. Erdman, T.C.T. Peret, C. Burns, T.G. Ksiazek, P.E. Rollin, A. Sanchez, S. Liffick, B. Holloway, J. Limor, K. McCaustland, M. Olsen-Rasmussen, R. Fouchier, S. Günther, A.D.H.E. Osterhaus, C. Drosten, M.A. Pallansch, L.J. Anderson, W.J. Bellini, Characterization of a novel coronavirus associated with severe acute respiratory syndrome, Science 300 (2003) 1394–1399, http://dx.doi.org/10.1126/science.1085952.

[6] T.G. Ksiazek, D. Erdman, C.S. Goldsmith, S.R. Zaki, T. Peret, S. Emery, S. Tong, C. Urbani, J.A. Comer, W. Lim, P.E. Rollin, S.F. Dowell, A.-E. Ling, C.D. Humphrey, W.-J. Shieh, J. Guarner, C.D. Paddock, P. Rota, B. Fields, J. DeRisi, J.-Y. Yang, N. Cox, J.M. Hughes, J.W. LeDuc, W.J. Bellini, L.J. Anderson, A novel coronavirus associated with severe acute respiratory syndrome, N. Engl. J. Med. 348 (2003) 1953–1966, http://dx.doi.org/10.1056/nejmoa030781.

[7] A.M. Zaki, S. van Boheemen, T.M. Bestebroer, A.D.M.E. Osterhaus, R.A.M. Fouchier, Isolation of a novel coronavirus from a man with pneumonia in Saudi Arabia, N. Engl. J. Med. 367 (2012) 1814–1820, http://dx.doi.org/10.1056/nejmoa1211721.

[8] R.J. de Groot, S.C. Baker, R.S. Baric, C.S. Brown, C. Drosten, L. Enjuanes, R.A.M. Fouchier, M. Galiano, A.E. Gorbalenya, Z.A. Memish, S. Perlman, L.L.M. Poon, E.J. Snijder, G.M. Stephens, P.C.Y. Woo, A.M. Zaki, M. Zambon, J. Ziebuhr, Middle east respiratory syndrome coronavirus (MERS-CoV): Announcement of the coronavirus study group, J. Virol. 87 (2013) 7790–7792, http://dx.doi.org/10.1128/jvi.01244-13.

[9] Center, Center for systems science and engineering, COVID-19 dashboard by the center for systems and engineering at johns hopkins university, Lancet Infect. Dis. 19 (2021) 533–534, https://coronavirus.jhu.edu/map.html.

[10] M. Gui, W. Song, H. Zhou, J. Xu, S. Chen, Y. Xiang, X. Wang, Cryo-electron microscopy structures of the SARS-CoV spike glycoprotein reveal a prerequisite conformational state for receptor binding, Cell Res. 27 (2017) 119–129, http://dx.doi.org/10.1038/cr.2016.152.

[11] L. Zhang, C.B. Jackson, H. Mou, A. Ojha, H. Peng, B.D. Quinlan, E.S. Rangarajan, A. Pan, A. Vanderheiden, M.S. Suthar, W. Li, T. Izard, C. Rader, M. Farzan, H. Choe, SARS-CoV-2 spike-protein D614g mutation increases virion spike density and infectivity, Nature Commun. 11 (2020) 1–9, http://dx.doi.org/10.1038/s41467-020-19808-4.

[12] C. Shen, S.A. Bradford, Why are viruses spiked? MSphere 6 (2021) 17–20, http://dx.doi.org/10.1128/msphere.01339-20.

[13] B.A. Taha, N. Ali, N.M. Sapiee, M.M. Fadhel, R.M. Mat Yeh, N.N. Bachok, Y. Al Mashhadany, N. Arsad, Comprehensive review tapered optical fiber configurations for sensing application: Trend and challenges, Biosensors 11 (2021) 253, http://dx.doi.org/10.3390/bios11080253.

[14] L. Zhang, W.Q. Yan, Deep learning methods for virus identification from digital images, in: International Conference Image and Vision Computing New Zealand, Vol. 2020, 2020, pp. 6–11, http://dx.doi.org/10.1109/IVCNZ51579.2020.9290670.

[15] M. Laue, A. Kauter, T. Hoffmann, L. Möller, J. Michel, A. Nitsche, Morphometry of SARS-CoV and SARS-CoV-2 particles in ultrathin plastic sections of infected vero cell cultures, Sci. Rep. 11 (2021) 1–11, http://dx.doi.org/10.1038/s41598-021-82852-7.

[16] B.W. Neuman, G. Kiss, A.H. Kunding, D. Bhella, M.F. Baksh, S. Connelly, B. Droese, J.P. Klaus, S. Makino, S.G. Sawicki, S.G. Siddell, D.G. Stamou, I.A. Wilson, P. Kuhn, M.J. Buchmeier, A structural analysis of M protein in coronavirus assembly and morphology, J. Struct. Biol. 174 (2011) 11–22, http://dx.doi.org/10.1016/j.jsb.2010.11.021.

[17] Z. Ke, J. Oton, K. Qu, M. Cortese, V. Zila, L. McKeane, T. Nakane, J. Zivanov, C.J. Neufeldt, B. Cerikan, J.M. Lu, J. Peukes, X. Xiong, H.G. Kräusslich, S.H.W. Scheres, R. Bartenschlager, J.A.G. Briggs, Structures and distributions of SARS-CoV-2 spike proteins on intact virions, Nature 588 (2020) 498–502, http://dx.doi.org/10.1038/s41586-020-2665-2.

[18] B.A. Taha, Y. Al Mashhadany, M.H.H. Mokhtar, M.S.D. Bin Zan, N. Arsad, An analysis review of detection coronavirus disease 2019 (Covid-19) based on biosensor application, Sensors (Switzerland) 20 (2020) 1–29, http://dx.doi.org/10.3390/s20236764.

[19] B.A. Taha, Y. Al Mashhadany, N.N. Bachok, A. Ashrif A. Bakar, M.H. Hafiz Mokhtar, M.S. Dzulkefly Bin Zan, N. Arsad, Detection of covid-19 virus on surfaces using photonics: Challenges and perspectives, Diagnostics 11 (2021) 1119, http://dx.doi.org/10.3390/diagnostics11061119.

[20] B.A. Taha, Perspectives of photonics technology to diagnosis COVID–19 viruses: A short review, J. Appl. Sci. Nanotechnol. 1 (2021) 1–6, http://dx.doi.org/10.53293/jasn.2021.11016.

[21] R. Achanta, A. Shaji, K. Smith, A. Lucchi, P. Fua, S. Süsstrunk, S. Susstrunk, S. Süsstrunk, SLIC superpixels compared to state-of-the-art superpixel methods, IEEE Trans. Pattern Anal. Mach. Intell. 34 (2012) 2274–2282, http://dx.doi.org/10.1109/TPAMI.2012.120.

[22] A. Aghamohammadi, M.C. Ang, E.A. Sundararajan, K.W. Ng, M. Mogharrebi, S.Y. Banihashem, Correction: A parallel spatiotemporal saliency and discriminative online learning method for visual target tracking in aerial videos, PLoS ONE 13 (2018) 1–19, http://dx.doi.org/10.1371/journal.pone.0195418, (PLoS ONE (2018) 13:2(e0192246) doi:10.1371/journal.pone.0192246).

[23] R.J. Al-Azawi, Q.S. Al-Jubouri, Y.A. Mohammed, Enhanced algorithm of superpixel segmentation using simple linear iterative clustering, in: Proceedings - International Conference on Developments in ESystems Engineering, DeSE, 2019, pp. 160–163, http://dx.doi.org/10.1109/DeSE.2019.00038.

[24] T.H. Yuan, F.H. Hashim, W.M.D.W. Zaki, A.B. Huddin, An automated 3D scanning algorithm using depth cameras for door detection, in: Proceedings - 2015 International Electronics Symposium: Emerging Technology in Electronic and Information, IES 2015, 2016, pp. 58–61, http://dx.doi.org/10.1109/ELECSYM.2015.7380814.

[25] M.F. Ibrahim, A.B. Huddin, M.H. Mohd Zaman, A. Hussain, S.N. Anual, An enhanced frontier strategy with global search target-assignment approach for autonomous robotic area exploration, Int. J. Adv. Technol. Eng. Explor. 8 (2021) 283–291, http://dx.doi.org/10.19101/IJATEE.2020.762170.

[26] N.S.M. Zamani, W.M.D.W. Zaki, A.B. Huddin, A. Hussain, H.A. Mutalib, A. Ali, Automated pterygium detection using deep neural network, IEEE Access 8 (2020) 191659–191672, http://dx.doi.org/10.1109/ACCESS.2020.3030787.

[27] S.M. Ashhar, S.S. Mokri, A.A.A. Rahni, A.B. Huddin, N. Zulkarnain, N.A. Azmi, T. Mahaletchumy, Comparison of deep learning convolutional neural network (CNN) architectures for CT lung cancer classification, Int. J. Adv. Technol. Eng. Explor. 8 (2021) 126–134, http://dx.doi.org/10.19101/IJATEE.2020.S1762126.

[28] K.S. Choi, K.W. Oh, Subsampling-based acceleration of simple linear iterative clustering for superpixel segmentation, Comput. Vis. Image Underst. 146 (2016) 1–8, http://dx.doi.org/10.1016/j.cviu.2016.02.018.

[29] M. Angulakshmi, G.G. Lakshmi Priya, Walsh Hadamard transform for simple linear iterative clustering (SLIC) superpixel based spectral clustering of multimodal MRI brain tumor segmentation, Irbm 40 (2019) 253–262, http://dx.doi.org/10.1016/j.irbm.2019.04.005.

[30] A. Albayrak, G. Bilgin, Automatic cell segmentation in histopathological images via two-staged superpixel-based algorithms, Med. Biol. Eng. Comput. 57 (2019) 653–665, http://dx.doi.org/10.1007/s11517-018-1906-0.

[31] J. Wu, C. Liu, B. Li, Texture-aware and structure-preserving superpixel segmentation, Comput. Graph. (Pergamon) 94 (2021) 152–163, http://dx.doi.org/10.1016/j.cag.2020.12.002.

[32] X. Wei, Q. Yang, Y. Gong, N. Ahuja, M.H. Yang, Superpixel hierarchy, IEEE Trans. Image Process. 27 (2018) 4838–4849, http://dx.doi.org/10.1109/TIP.2018.2836300.

[33] B. Han, J. Yin, X. Luo, H. Qv, A hierarchical superpixel aggregation model for hyperspectral image, in: International Geoscience and Remote Sensing Symposium, Vol. 2017, IGARSS, 2017, pp. 3767–3770, http://dx.doi.org/10.1109/IGARSS.2017.8127819.

[34] N. Zhu, D. Zhang, W. Wang, X. Li, B. Yang, J. Song, X. Zhao, B. Huang, W. Shi, R. Lu, P. Niu, F. Zhan, X. Ma, D. Wang, W. Xu, G. Wu, G.F. Gao, W. Tan, A novel coronavirus from patients with Pneumonia in China, 2019, N. Engl. J. Med. 382 (2020) 727–733, http://dx.doi.org/10.1056/nejmoa2001017.

[35] J. Abraham, Passive antibody therapy in COVID-19, Nat. Rev. Immunol. 20 (2020) 401–403, http://dx.doi.org/10.1038/s41577-020-0365-7.

[36] F. Li, Receptor recognition mechanisms of coronaviruses: a decade of structural studies, J. Virol. 89 (2015) 1954–1964, http://dx.doi.org/10.1128/jvi.02615-14.

[37] B. Turoňová, M. Sikora, C. Schürmann, W.J.H. Hagen, S. Welsch, F.E.C. Blanc, S. von Bülow, M. Gecht, K. Bagola, C. Hörner, G. van Zandbergen, J. Landry, N.T.D. de Azevedo, S. Mosalaganti, A. Schwarz, R. Covino, M.D. Mühlebach, G. Hummer, J.K. Locker, M. Beck, In situ structural analysis of SARS-CoV-2 spike reveals flexibility mediated by three hinges, Science 370 (2020) 203–208, http://dx.doi.org/10.1126/science.abd5223.

[38] M. Alejandra Tortorici, A.C. Walls, Y. Lang, C. Wang, Z. Li, D. Koerhuis, G.J. Boons, B.J. Bosch, F.A. Rey, R.J. de Groot, D. Veesler, Structural basis for human coronavirus attachment to sialic acid receptors, Nat. Struct. Mol. Biol. 26 (2019) 481–489, http://dx.doi.org/10.1038/s41594-019-0233-y.

[39] C.A. Beaudoin, A.R. Jamasb, A.F. Alsulami, L. Copoiu, A.J. van Tonder, S. Hala, B.P. Bannerman, S.E. Thomas, S.C. Vedithi, P.H.M. Torres, T.L. Blundell, Predicted structural mimicry of spike receptor-binding motifs from highly pathogenic human coronaviruses, Comput. Struct. Biotechnol. J. 19 (2021) 3938–3953, http://dx.doi.org/10.1016/j.csbj.2021.06.041.

[40] S. Klein, M. Cortese, S.L. Winter, M. Wachsmuth-Melm, C.J. Neufeldt, B. Cerikan, M.L. Stanifer, S. Boulant, R. Bartenschlager, P. Chlanda, SARS-CoV-2 structure and replication characterized by in situ cryo-electron tomography, Nature Commun. 11 (2020) 1–10, http://dx.doi.org/10.1038/s41467-020-19619-7.

[41] J. Shang, Y. Wan, C. Luo, G. Ye, Q. Geng, A. Auerbach, F. Li, Cell entry mechanisms of SARS-CoV-2, in: Proceedings of the National Academy of Sciences of the United States of America, Vol. 117, 2020, http://dx.doi.org/10.1073/pnas.2003138117.

[42] G. Zhou, Q. Zhao, Perspectives on therapeutic neutralizing antibodies against the novel coronavirus sars-cov-2, Int. J. Biol. Sci. 16 (2020) 1718–1723, http://dx.doi.org/10.7150/ijbs.45123.

[43] Y. Huang, C. Yang, X. feng Xu, W. Xu, S. wen Liu, Structural and functional properties of SARS-CoV-2 spike protein: potential antivirus drug development for COVID-19, Acta Pharmacol. Sin. 41 (2020) 1141–1149, http://dx.doi.org/10.1038/s41401-020-0485-4.

[44] Y. Yuan, W. Zhang, H. Yu, Z. Zhu, Superpixels with content-adaptive criteria, IEEE Trans. Image Process. 30 (2021) 7702–7716, http://dx.doi.org/10.1109/TIP.2021.3108403.

[45] A. Ibrahim, E.-S.M. El-Kenawy, Image segmentation methods based on superpixel techniques: A survey, J. Comput. Sci. Inf. Syst. 2020 (2020) 1–10, www.jcsis.org/.

[46] C.H. Wu, H.H. Chang, Superpixel-based image noise variance estimation with local statistical assessment, Eurasip J. Image Video Process. 2015 (2015) 1–12, http://dx.doi.org/10.1186/s13640-015-0093-2.

[47] L. Yao, S. Muhammad, A novel technique for analysing histogram equalized medical images using superpixels, Comput. Assist. Surg. 24 (2019) 53–61, http://dx.doi.org/10.1080/24699322.2018.1560100.

[48] R. Achanta, A. Shaji, K. Smith, A. Lucchi, P. Fua, S. Susstrunk, SLIC superpixels, 2010, http://dx.doi.org/10.1109/TPAMI.2012.120.

[49] L.M. Abualigah, A.T. Khader, M.A. Al-Betar, Multi-objectives-based text clustering technique using K-mean algorithm, in: Proceedings - CSIT 2016: 2016 7th International Conference on Computer Science and Information Technology, 2016, pp. 12–17, http://dx.doi.org/10.1109/CSIT.2016.7549464.

[50] C. Yang, L. Bruzzone, H. Zhao, Y. Tan, R. Guan, Superpixel-based unsupervised band selection for classification of hyperspectral images, IEEE Trans. Geosci. Remote Sens. 56 (2018) 7230–7245, http://dx.doi.org/10.1109/TGRS.2018.2849443.

[51] K.V. Rani, S.J. Jawhar, Superpixel with nanoscale imaging and boosted deep convolutional neural network concept for lung tumor classification, Int. J. Imaging Syst. Technol. 30 (2020) 899–915, http://dx.doi.org/10.1002/ima.22422.

[52] S. Ji, B. Wei, Z. Yu, G. Yang, Y. Yin, A new multistage medical segmentation method based on superpixel and fuzzy clustering, Comput. Math. Methods Med. 2014 (2014) http://dx.doi.org/10.1155/2014/747549.

[53] K. Smith, R. Achanta, G. Knott, P. Fua, Supervoxel-based segmentation of EM image stacks with learned shape features, Scanning Electron Microsc. 31 (2010) 1–12.

[54] Z. Chen, B. Guo, C. Lib, H. Liu, Review on superpixel generation algorithms based on clustering, in: Proceedings of 2020 IEEE 3rd International Conference on Information Systems and Computer Aided Education, ICISCAE 2020, 2020, pp. 532–537, http://dx.doi.org/10.1109/ICISCAE51034.2020.9236851.

[55] X. Luo, Image compression via K-means and SLIC superpixel approaches, 71 (2016) 1008–1012. http://dx.doi.org/10.2991/icmmita-16.2016.185.

[56] X. Ren, J. Malik, Learning a classification model for segmentation, in: Proceedings of the IEEE International Conference on Computer Vision, Vol. 1, 2003, pp. 10–17, http://dx.doi.org/10.1109/iccv.2003.1238308.

[57] T. Toth, T. Balassa, N. Bara, F. Kovacs, A. Kriston, C. Molnar, L. Haracska, F. Sukosd, P. Horvath, Environmental properties of cells improve machine learning-based phenotype recognition accuracy, Sci. Rep. 8 (2018) 1–9, http://dx.doi.org/10.1038/s41598-018-28482-y.

[58] A. Yang, C.T. Veal, D.T. Anderson, G.J. Scott, Recognizing image objects by relational analysis using heterogeneous superpixels and deep convolutional features, 2019, pp. 1–10, http://arxiv.org/abs/1908.00669.

[59] Y. Chen, Y. Zhang, J. Yang, Q. Cao, G. Yang, J. Chen, H. Shu, L. Luo, J.L. Coatrieux, Q. Feng, Curve-like structure extraction using minimal path propagation with backtracking, IEEE Trans. Image Process. 25 (2016) 988–1003, http://dx.doi.org/10.1109/TIP.2015.2496279.

[60] M. Soltaninejad, G. Yang, T. Lambrou, N. Allinson, T.L. Jones, T.R. Barrick, F.A. Howe, X. Ye, Automated brain tumour detection and segmentation using superpixel-based extremely randomized trees in FLAIR MRI, Int. J. Comput. Assist. Radiol. Surg. 12 (2017) 183–203, http://dx.doi.org/10.1007/s11548-016-1483-3.

[61] D. Wrapp, N. Wang, K.S. Corbett, J.A. Goldsmith, C.L. Hsieh, O. Abiona, B.S. Graham, J.S. McLellan, Cryo-EM structure of the 2019-nCoV spike in the prefusion conformation, Science 367 (2020) 1260–1263, http://dx.doi.org/10.1126/science.aax0902.

[62] A.C. Walls, Y.J. Park, M.A. Tortorici, A. Wall, A.T. McGuire, D. Veesler, Structure, function, and antigenicity of the SARS-CoV-2 spike glycoprotein, Cell 181 (2020) 281–292, http://dx.doi.org/10.1016/j.cell.2020.02.058, e6.

[63] M. Hoffmann, H. Kleine-Weber, S. Schroeder, N. Krüger, T. Herrler, S. Erichsen, T.S. Schiergens, G. Herrler, N.H. Wu, A. Nitsche, M.A. Müller, C. Drosten, S. Pöhlmann, SARS-CoV-2 cell entry depends on ACE2 and TMPRSS2 and is blocked by a clinically proven protease inhibitor, Cell 181 (2020) 271–280, http://dx.doi.org/10.1016/j.cell.2020.02.052, e8.

[64] A. Bal, G. Destras, A. Gaymard, M. Bouscambert-Duchamp, M. Valette, V. Escuret, E. Frobert, G. Billaud, S. Trouillet-Assant, V. Cheynet, K. Brengel-Pesce, F. Morfin, B. Lina, L. Josset, Molecular characterization of SARS-CoV-2 in the first COVID-19 cluster in France reveals an amino acid deletion in nsp2 (asp268del), Clin. Microbiol. Infect. 26 (2020) 960–962, http://dx.doi.org/10.1016/j.cmi.2020.03.020.

[65] Y. Pathak, P.K. Shukla, A. Tiwari, S. Stalin, S. Singh, Deep transfer learning based classification model for COVID-19 disease, Irbm (2020) http://dx.doi.org/10.1016/j.irbm.2020.05.003.

[66] A. Ibrahim, M. Salem, H.A. Ali, Block-based illumination-invariant representation for color images, Ain Shams Eng. J. 9 (2018) 917–926, http://dx.doi.org/10.1016/j.asej.2016.04.011.

[67] H. Akkiz, Implications of the novel mutations in the SARS-CoV-2 genome for transmission, disease severity, and the vaccine development, Front. Med. 8 (2021) 1–10, http://dx.doi.org/10.3389/fmed.2021.636532.

[68] D. Mercatelli, F.M. Giorgi, Geographic and genomic distribution of SARS-CoV-2 mutations, Front. Microbiol. 11 (2020) 1–13, http://dx.doi.org/10.3389/fmicb.2020.01800.

[69] J.V. Davis, I. Dhillon, Differential entropic clustering of multivariate Gaussians, Adv. Neural Inf. Process. Syst. (2007) 337–344, http://dx.doi.org/10.7551/mitpress/7503.003.0047.

[70] F. Colavita, D. Lapa, F. Carletti, E. Lalle, L. Bordi, P. Marsella, E. Nicastri, N. Bevilacqua, M.L. Giancola, A. Corpolongo, G. Ippolito, M.R. Capobianchi, C. Castilletti, M.A. Abbonizio, C. Agrati, F. Albarello, G. Amadei, A. Amendola, M. Antonini, R. Barbaro, B. Bartolini, M. Benigni, V. Bordoni, M. Branca, P. Campioni, C. Caporale, I. Caravella, R. Chiappini, C. Ciaralli, M. Cristofaro, S. Curiale, A. D'Abramo, C. Dantimi, A. de Angelis, G. de Angelis, R. Di Lorenzo, F. Di Stefano, F. Ferraro, L. Fiorentini, A. Frustaci, P. Gallì, G. Garotto, F. Giansante, E. Giombini, M.C. Greci, S. Lanini, L. Lepore, A. Lucia, F. Lufrani, M. Macchione, A. Marani, L. Marchioni, A. Mariano, M.C. Marini, M. Maritti, G. Matusali, S. Meschi, F. Messina, C. Montaldo, S. Murachelli, E. Nicastri, R. Noto, C. Palazzolo, E. Pallini, V. Passeri, F. Pelliccioni, A. Petrecchia, A. Petrone, N. Petrosillo, E. Pianura, M. Pisciotta, S. Pittalis, C. Proietti, V. Puro, G. Rinonapoli, M. Rueca, A. Sacchi, F. Sanasi, C. Santagata, S. Scarcia, V. Schininà, P. Scognamiglio, L. Scorzolini, G. Stazi, F. Vaia, F. Vairo, M.B. Valli, SARS-CoV-2 isolation from ocular secretions of a patient with COVID-19 in Italy with prolonged viral RNA detection, Ann. Intern. Med. 173 (2020) 242–243, http://dx.doi.org/10.7326/M20-1176.

[71] V. Thiel, K.A. Ivanov, Á. Putics, T. Hertzig, B. Schelle, S. Bayer, B. Weiß brich, E.J. Snijder, H. Rabenau, H.W. Doerr, A.E. Gorbalenya, J. Ziebuhr, Mechanisms and enzymes involved in SARS coronavirus genome expression, J. Gen. Virol. 84 (2003) 2305–2315, http://dx.doi.org/10.1099/vir.0.19424-0.